ELSEVIER

Journal of Hydrology 231–232 (2000) 244–254

Journal of Hydrology

www.elsevier.com/locate/jhydrol

Soil water content dependent wetting front characteristics in sands

T.W.J. Bauters[a], D.A. DiCarlo[b], T.S. Steenhuis[a,*], J.-Y. Parlange[a]

[a]*Department of Agricultural and Biological Engineering, Cornell University, Ithaca, NY 14853, USA*
[b]*Department of Petroleum Engineering, Stanford University, Stanford, CA 94305, USA*

Received 2 April 1999; accepted 13 August 1999

Abstract

The initial soil water content affects wetting front instability. A series of experiments were conducted where water was infiltrated into a 20/30 sand with initial volumetric water contents of 0, 0.005, 0.01, 0.015, 0.02, 0.03, 0.04 and 0.047 cm^3/cm^3. Both water content and matric potential were measured. Water content was measured with Synchrotron X-rays at the Cornell High Energy Synchrotron Source (CHESS) and matric potential with fast responding tensiometers. The flow field changed gradually from unstable fingered flow at 0% initial water content to a wetting pattern that can be described with Richards' equation without hysteresis. For unstable flow, the matric potential and water content decreased a short distance behind the wetting front. Except in the initially dry soil, the finger pattern began to widen immediately after infiltration. The pressure and water content of the wetting front were hyperbolically related to the initial water content. In general, this research showed that in coarse soils when an unstable wetting front occurs both the matric potential and water content drop behind the wetting front while, when a stable Richards' type wetting front forms, the matric potential and water content increase (slightly) behind the wetting front. © 2000 Elsevier Science B.V. All rights reserved.

Keywords: Vadose zone; Unstable front; Fingered flow; Infiltration

1. Introduction

Since the early 1960s, the occurrence of unstable fingered flow has been observed in initially dry sandy soil by Miller and Gardner (1962), Peck (1965) and Hill and Parlange (1972). Theory for unstable fingered wetting fronts was developed by Raats (1973), Parlange and Hill (1976), Glass et al. (1989), Selker et al. (1992b), Kapoor (1996) and Yao and Hendrickx (1996). Bauters et al. (1998) showed that the finger-like pattern in water repellent soil had many similarities with unstable wetting fronts in air dry coarse-grained soils. Despite the abundance of research in wetting front behavior for initially dry soil, studies of unstable flow in initially moist coarse or hydrophobic soils (Ritsema et al., 1998) are very limited: Diment and Watson (1982) carried out infiltration experiments in sands with different water contents and reported that water contents $>0.01\ cm^3/cm^3$ had an inhibiting effect on the development of frontal instability patterns in coarse sands. Liu et al. (1994) infiltrated water in experimental chambers with a dry soil on top and a capillary fringe at the bottom. They showed fingers, formed in the top section, increased in width in the capillary fringe. Because of the lack of systematic research in this area, the objective of this paper is to examine how initial water content affects infiltration patterns. Specifically, the wetting front behavior

* Corresponding author. Tel.: +1-607-255-2489; fax: +1-607-255-4080.

E-mail address: tss1@cornell.edu (T.S. Steenhuis).

0022-1694/00/$ - see front matter © 2000 Elsevier Science B.V. All rights reserved.
PII: S0022-1694(00)00198-0

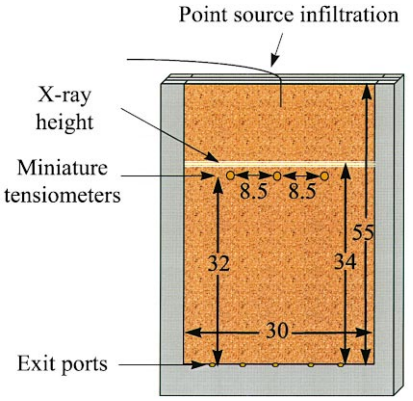

Fig. 1. The experimental chamber with point source infiltration, X-ray height, miniature tensiometers, and exit ports. All measurements are in cm.

and the water content and matric potential behind the wetting front will be characterized during water infiltration at different initial soil water contents between air dry and field capacity.

2. Materials and methods

Infiltration experiments were performed in the F-2 hutch of the Cornell High Energy Synchrotron Source (CHESS). Distilled water was applied as a point source at the surface in a 0.94 cm thick, 30 cm wide, and 55 cm long polycarbonate chamber filled with clean, 20–30 (US sieve sizes; compared to sieve openings of 0.850/0.600 mm as upper/lower limit, respectively) quartz sand (Unimin Corporation[1]) (Fig. 1) with initial water contents ranging from 0 to 0.047 cm^3/cm^3. Excess water drained out of the chamber through a manifold of five fluid ports. 0.005% FD&C blue #1 (Warner–Jenkinson Co, Inc.[1]) was dissolved in the infiltrating water to make the wetting front more visible.

Depending on the initial water content, different procedures were used for filling the chamber. For the 0 cm^3/cm^3 volumetric water content, sand was added by pouring it continuously through a number of randomized screens. For the 0.047 cm^3/cm^3 water content, the same filling procedure was used but then the chamber was saturated from the bottom at a flow rate of 3 $cm^3\ min^{-1}$. Once the water level reached the top, it was drained to a residual water content of 0.047 cm^3/cm^3 (measured with X-rays and confirmed gravimetrically in a separate experiment). For the remaining water contents, 0.005, 0.01, 0.015, 0.02, 0.03 and 0.04 cm^3/cm^3, 1.73 kg of 20/30 sand was mixed manually with the 5, 10, 15, 20, 30 and 40 ml distilled water, respectively. The chamber was filled in layers of 3 cm and then tamped by raising and dropping five times a polycarbonate board (29.5 cm wide, 70 cm tall, and 0.47 cm thick) 10 cm above the sand. This procedure resulted in a smooth packing and a repeatable density of 1.73 g/cm^3. The tamping caused the chamber to bulge in the middle which affected X-ray attenuation. The procedure to compensate for the chamber's thickness variation and determination of the moisture content is discussed later.

Infiltrating experiments were performed by injecting distilled water at a rate of 2 $cm^3\ min^{-1}$ through a hypodermic needle located near the sand surface. In the experiments in which small fingers formed, up to three infiltrations were carried out at different locations in the same packed chamber.

Matric potentials were measured with three fast responding miniature tensiometers (Selker et al., 1992a) positioned flush with the wall, 8.5 cm apart and 32 cm from the bottom (Fig. 1). The tensiometers consisted of a body, machined out of brass, and a stainless steel porous plate (20 μm pore size). The tensiometers were filled with degassed, distilled water and connected with nylon tubing through a three-way valve. The three outlets were connected either to a calibration tube, a pressure transducer, or a 60 cc syringe, holding the degassed, distilled water for filling the tensiometers. The voltages of the pressure transducers were filtered, amplified, integrated over 1 s and electronically recorded. Before each experiment, the tensiometers were calibrated by varying the height in the calibration tube with known water levels using the syringe.

Water content was measured with high intensity X-rays. The initial white X-ray beam reflected off a Si-Crystal, producing a beam with a fundamental energy of 25 keV. The beam coming in the F-2 hutch was collimated with tantalum slits to a size of 1 mm vertical by 10 mm horizontal. The beam passed through 53 cm of open air, an argon filled ion chamber, 53 cm

[1] Mentioning of product names does not suggest an endorsement of the product.

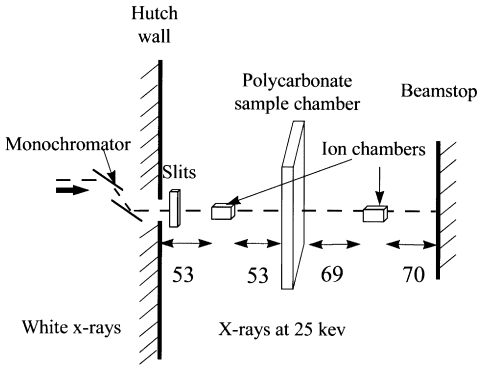

Fig. 2. A schematic of the experimental setup at the F-2 hutch of CHESS. The monochrometer transforms the white X-ray beam into a beam with a fundamental energy of 25 keV. Ion chambers measure the total intensity of the X-ray beam (no energy resolution). The sample chamber is mounted on a movable platform allowing measurements from many different positions within the chamber. All measurements are in cm.

of open air, the sample chamber, another argon filled ion chamber at 69 cm from the sample chamber, and 70 cm more open air before hitting the beam stop (Fig. 2). The details of this setup are discussed in DiCarlo et al. (1997).

The chamber was mounted on a movable *x*, *y* platform so that measurements could be taken at any position within the chamber. The horizontal scans in the chamber were taken every 5 mm for all experiments. Stationary data to document the water content within the finger were collected 2 cm above the tensiometers (34 cm above the chamber bottom) (Fig. 1). The finger widths were calculated from the horizontal scans at a height of 34 cm. The finger width for the unstable fingered flow regime was taken at the maximum water content while, for the stable flow cases, the width of the wetting front was measured where the water content became constant. The width at the tail of the finger was also taken at a height of 34 cm, just before the infiltration was stopped.

Infiltration patterns were recorded with a CCD camera, connected to a Panasonic AG 6720 video cassette recorder. The blue dye aided in better visualization of the infiltrating water. The view of the lower 15 cm was obstructed by the X-ray detector. In addition, space limitations in the F-2 hutch only allowed us to record the wetting front pattern approximately 15 cm from the top. The recorded images were digitized with a frame grabber from Data Translations. Global Labs Imaging software was used in transferring the grabbed images to tiff-format which were then imported into Adobe Photoshop 4.0 to obtain the wetting front positions. In Photoshop, the images were first filtered with a median filter to reduce the noise, then thresholded at gray level 100, and transformed to a black and white image. All the images were then combined to make a time series of the wetting front location (Fig. 3). The velocities of the tip of the wetting front were calculated from these images.

Determination of the water content by X-ray attenuation requires a precise knowledge of the thickness of the chamber. Since the chamber width was only affected by the tamping and did not change during the experiment, we can use the initial X-ray scan before the water was infiltrated to find the chamber width in the experiments where tamping was used to fill the chamber (0.005, 0.01, 0.015, 0.02, 0.03 and 0.04 cm^3/cm^3). Using and adjusting Eq. (2) from DiCarlo et al. (1997) we find the distance of sand and initial water traversed (X) by the X-rays as:

$$X(x) = -\frac{A_i(x) - A_0}{U_s(1-n) + U_w\theta_i} \quad (1)$$

where $A_i(x)$ is the measured X-ray attenuation for sand and initial water as a function of the horizontal position x; A_0 the X-ray attenuation for empty chamber; U_s the attenuation constant of sand per unit width; n the porosity; $(1-n)$ is volumetric sand content; U_w the attenuation constant of water per unit width; θ_i the initial volumetric water content of sand.

In a separate experiment with a rigid sand filled chamber, the porosity was measured as 0.348 cm^3/cm^3 which is identical to that of Schroth et al. (1996). Since there was variation in local porosity due to arrangement of the sand grains within the 1 by 10 mm X-ray window, a second order polynomial was fitted through the width data obtained with Eq. (1) (Fig. 4 is an example for the 0.015 cm^3/cm^3 moist sand). The fitted distances, X, were used in all consequent calculations to find the water content at a particular location in the chamber as follows:

$$\theta = -\frac{A(x) - A_i(x)}{U_w X(x)} + \theta_i \quad (2)$$

where θ is the volumetric water content; A the X-ray

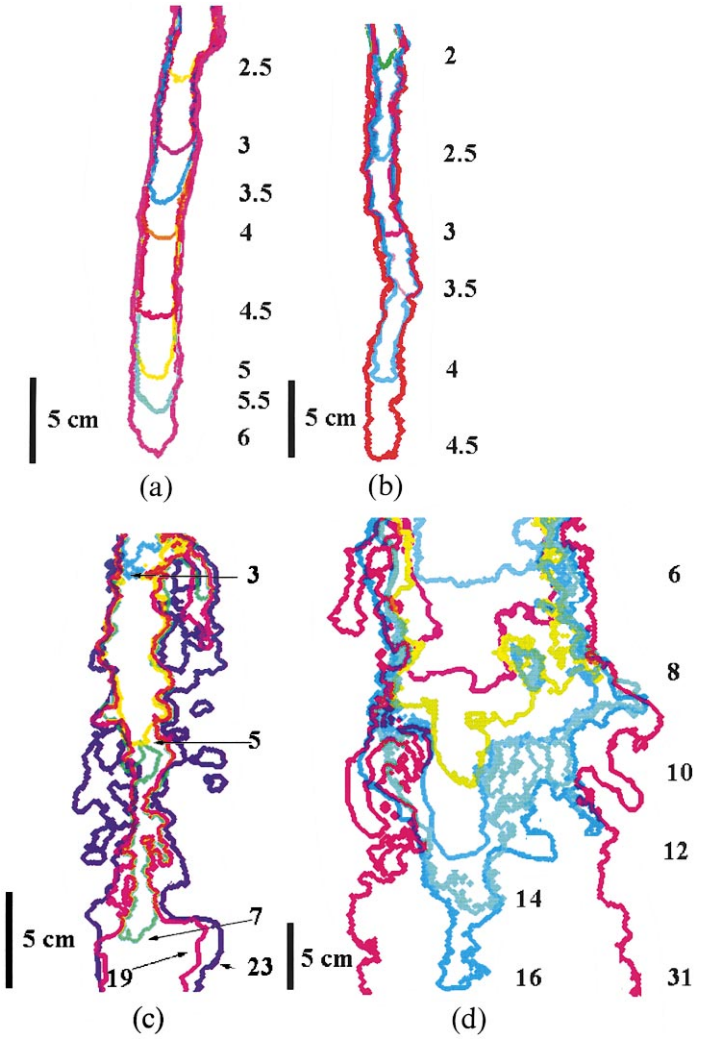

Fig. 3. (a) Tracings of the totally dry sand. The sequence of tracings are taken every 30 s. The numbers accompanying the tracings are the minutes after the infiltration started. A scale indicates 5 cm. (b) The advancing wetting front in the 0.01 cm^3/cm^3 moist sand. We notice that the infiltration front has a smaller width than in the totally dry case. (c) The advancing wetting front in the 0.02 cm^3/cm^3 initial moist sand pack. The tracings are depicted every 2 min. In addition, the latest tracing (after 23 min of infiltration) is shown. (d) Advancing wetting fronts in the 0.03 cm^3/cm^3 moist sand. Two-minute tracings are shown until the front reached the bottom of the visible area. In addition, the tracing of the front is depicted when the infiltration was stopped (after 31 min). (e) Advancing wetting fronts in the 0.04 cm^3/cm^3 initial moisture case. Two min tracings are shown until the front reached the bottom of the visible area. In addition, the front is depicted when the infiltration was stopped (after 32 min.). (f) The tracings of the wetting front when the chamber was imbibed from the bottom, or with a 0.047 cm^3/cm^3 (measured) initial moisture content. Tracings are depicted every 2 min.

attenuation with sand and both the initial and infiltrating water.

The static wetting branches of the soil characteristic curve were determined for the sands at different water contents. The moist sand was put into the chamber with the procedures described above. Water was imbibed from the bottom through the manifold with five fluid ports with a constant head of 5 cm from the bottom of the chamber. After 24 h of equilibration, the water contents were determined with the full field

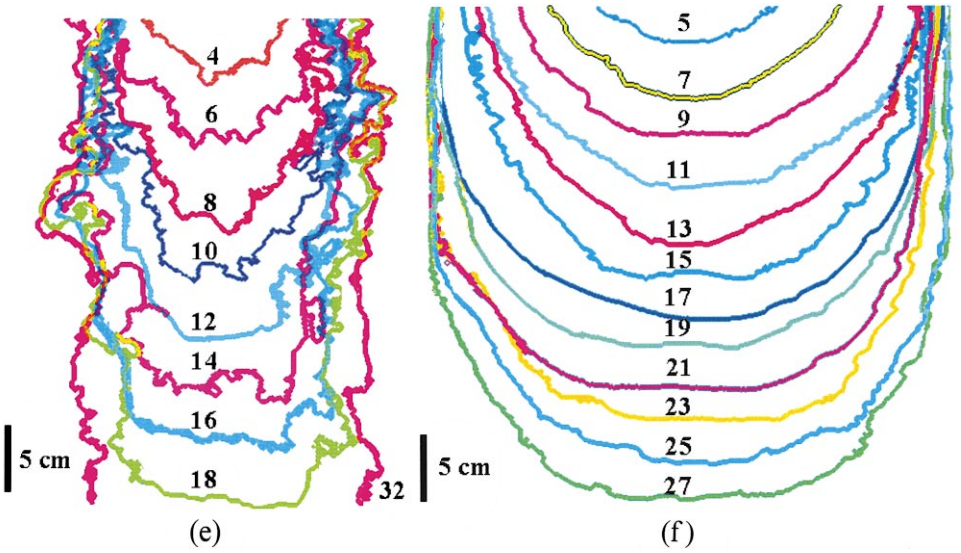

Fig. 3. (*continued*)

light visualization technique (Glass et al., 1989; DiCarlo et al., 1999) by placing the chamber in front of a bank of high frequency fluorescent lights. Light intensities were converted to water contents for five vertical transects (Bauters et al., 1998).

3. Results and discussion

3.1. Wetting front observation

There are several ways to determine if the wetting front pattern is unstable or not. The most convenient way is to visually observe the wetting pattern in time (Fig. 3). The finger width for the soils with 0 cm^3/cm^3 initial water content (Fig. 3a), 0.005 cm^3/cm^3 (not shown), and 0.01 cm^3/cm^3 (Fig. 3b) remains almost the same during the entire experiment. This is characteristic of an unstable wetting front. The finger width for the 0.01 cm^3/cm^3 initial water content was 1.25 cm, which was slightly smaller than that for the initially dry soil (Fig. 5). At 0.02 cm^3/cm^3 initial moisture content some widening occurred, but the typical finger structure was maintained (Fig. 3c). As we will discuss in more detail below, this finger was marginally unstable. For the 0.03 cm^3/cm^3 and higher initial moisture contents, the finger becomes much wider with time and at 0.047 cm^3/cm^3 fills the whole chamber (Fig. 3d–f). The widening of the finger for the 0.03 cm^3/cm^3 and higher initial water contents can be described using Richards' equation. Without hysteresis in the soil moisture characteristic curves, Richards' equation is unconditionally stable (Milly, 1988). For simplification, this type of wetting

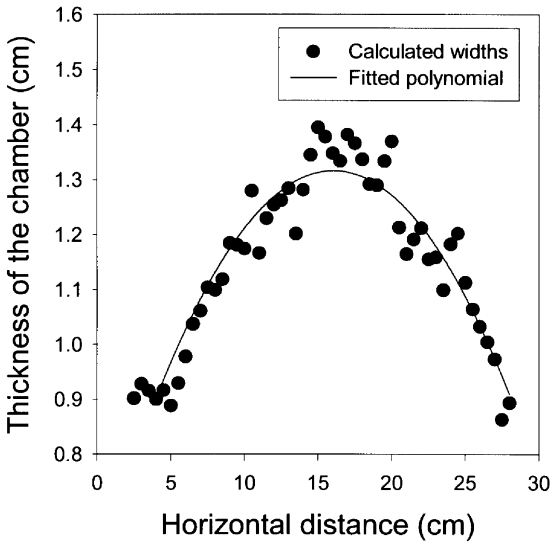

Fig. 4. The width of the chamber as calculated by Eq. (1) is depicted as well as the second degree polynomial that is fitted through the data.

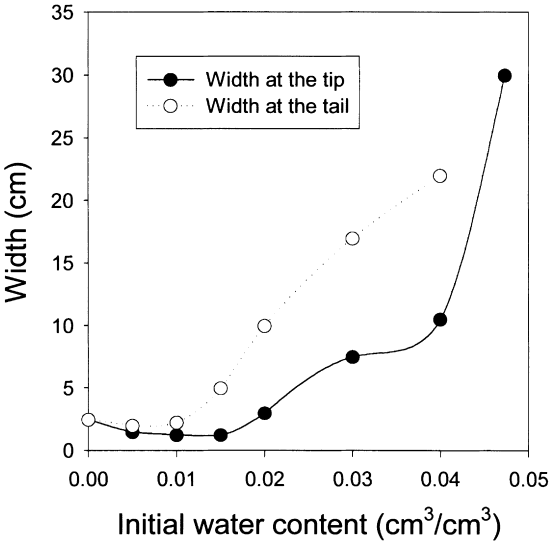

Fig. 5. The width at the beginning of the original infiltration and at the end of the infiltration is given versus the initial water content.

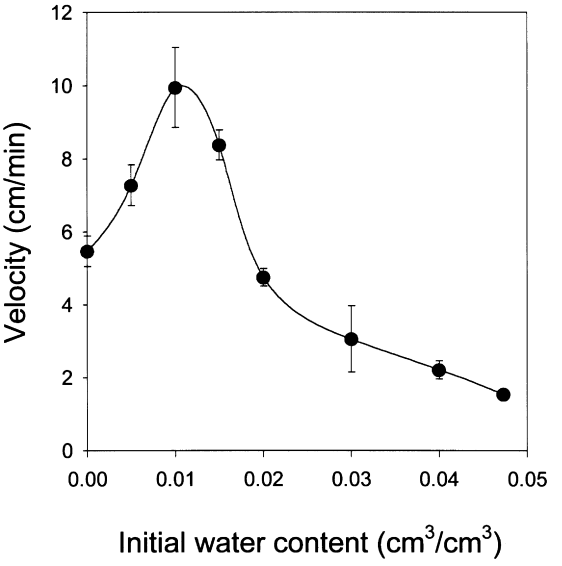

Fig. 6. The velocity at the wetting front versus the initial water content. The standard deviations are also plotted on the graph.

front will be referred to as "Richards' wetting front". For water infiltration resulting in the formation of unstable wetting fronts with fingers, the terms "unstable wetting front" and "fingered flow" will be used interchangeably.

The widths of fingers for all levels of initial water content are summarized in Fig. 5. The initial width decreased slightly with increasing initial water content up to 0.015 cm^3/cm^3 and then increased nearly exponentially. The final finger width (2.25 cm) for the initial 0.015 cm^3/cm^3 soil water content is very close to the initial width (2.5 cm) for the air dry soil during the 10 min infiltration. At initial water contents higher than 0.015 cm^3/cm^3, all fingers became wider than in the initially air dry soil. This increase was only minor for the 0.005 and 0.01 cm^3/cm^3 water contents. In general, the higher the initial water content the greater the increase in finger width. These results are consistent with DiCarlo et al. (1999) who studied the sideways expansion of fingers over an extended time period. They found that the finger width increased dramatically if the soil wetness was 0.02 cm^3/cm^3.

The wetting front velocity was approximately constant in our "observation window" at 15 cm from the top to approximately 15 cm from the bottom. The advance was much slower for the high water contents than for the low water contents. This is counterintuitive when classical Richards' type wetting front theory is considered (Fig. 6) that would suggest an increase in velocity with increasing water content. The highest velocity of 10 cm/min was measured at the 0.01 cm^3/cm^3 initial soil moisture content, which also corresponds to the smallest finger diameter (Figs. 3b and 6). The finger velocity in the air dry sand was approximately half of that at the 0.01 cm^3/cm^3 initial soil moisture content. There is a sixfold velocity decrease for the 0.01 and 0.047 cm^3/cm^3 initial water contents. As we will see next, the velocity is not only dependent on the finger width but also on the water content behind the wetting front.

3.2. Water and matric potential at and behind the wetting front

Raats (1973) theorized that, for unstable fronts, the matric potential should decrease behind the wetting front. Experimentally, Selker et al. (1992a) confirmed this for a coarse air dry 40/50 sand. Classical Richards' type flow shows a slight increase in matric potential behind the wetting front (Bruce and Klute, 1956). Our experimental data offer a good opportunity to examine this further.

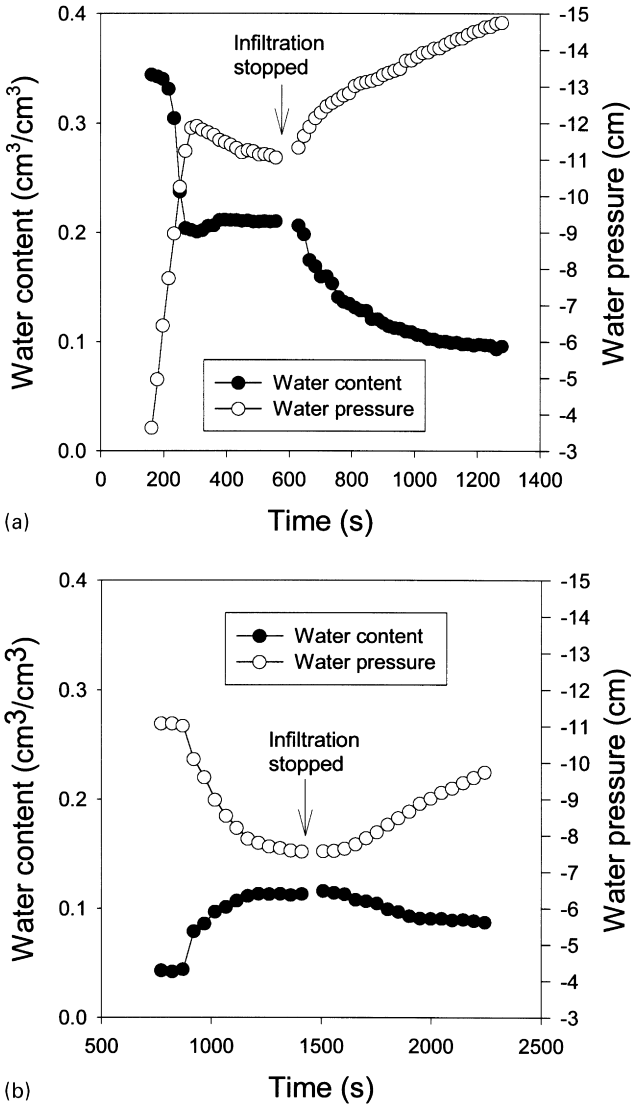

Fig. 7. (a) Time series for the dry soil, water content and pressures are depicted. Time starts when infiltration started. The data before the finger was hit is not plotted in the figure. (b) Time series for the 0.04 cm^3/cm^3 soil, water content and pressures are depicted. Time starts when infiltration started.

The change in matric potential and the water content at and behind the wetting front for all experiments are exemplified by two experiments: one at the dry end and one near field capacity. Fig. 7 shows the traces of both matric potential and water content at a location of 32 cm from the bottom (offset between both measuring points was corrected with the velocity) for water infiltrations into the initially air dry soil and into soil with the 0.04 cm^3/cm^3 initial water content. In the air dry soil (Fig. 7a), the finger tip reaches the tensiometer after 180 s of infiltration. The matric potential and water content at the wetting front are initially −3.6 cm and 0.345 cm^3/cm^3. The matric potential is equal to the water entry value and the water content is close to saturated water content of 0.348 cm^3/cm^3. Behind the tip, the water content stays initially saturated and then decreases rapidly to 0.20 cm^3/cm^3 at 252 s after the finger tip

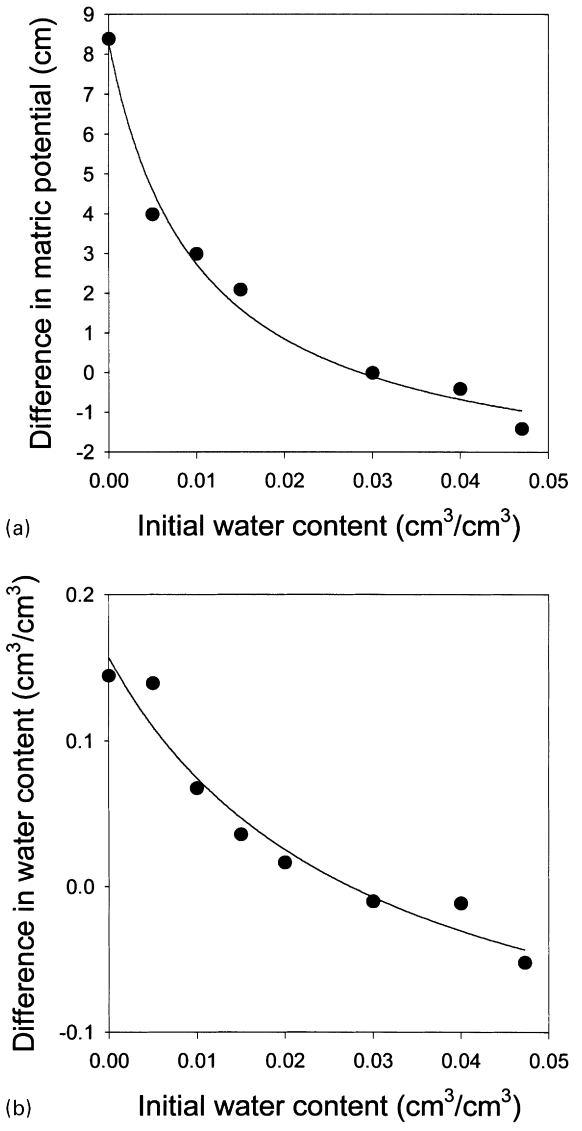

Fig. 8. (a) Matric potential difference between tip wetting pressure and tail pressure is plotted versus the initial water content. A hyperbolic decay function is fitted and shown on the graph. The hyperbolic decay function has a R^2 value of 99%. (b) Front moisture difference (initial volumetric water content at the tip of the wetting front minus the volumetric water content at the tail just before infiltration was stopped) versus the initial water content. The hyperbolic decay line is also depicted, and has a R^2 value of 95%.

reaches the bottom of the chamber. The moisture content remains approximately constant until the water is turned off at 558 s when the moisture content again starts to decrease. Thus, the matric potential behind the wetting front decreases to −11 cm and when the finger reaches the bottom of the chamber the matric potential increases. After the water application stops, the matric potential decreases too. For water infiltrating into the soil with the 0.04 cm^3/cm^3 water content (Fig. 7b), the matric potential and water content exhibit the typical Richards' pattern. The water content at the front is nearly 0.09 cm^3/cm^3 (unsaturated!) and then gradually increases to 0.12 cm^3/cm^3. The matric potential also increased slightly from −10.11 cm at the front to −7.6 cm at the time the water was turned off at 1410 s. Consequently, here for the same soil the initial unstable wetting front in dry soil becomes the Richards' type of wetting front when the soil is near field capacity. To examine how the change from unstable fingered flow to a Richards' type wetting front occurs, we will next compare the difference in matric potential and moisture content between the tip and tail for all initial water contents.

The difference in matric potential at the tip and the equilibrium value at the tail of the finger is plotted as a function of initial moisture contents in Fig. 8a. The equilibrium matric potential (called tail potential for short) was measured when the finger reached the bottom of the chamber or just before the infiltration was stopped. As discussed above, the difference in matric potential for the air dry sand, between the tip pressure and tail pressure, is 8.4 cm. At 0.01 cm^3/cm^3 initial water content, the pressure at the tip is only 3 cm higher than that in the tail. The difference in pressure becomes zero at 0.03 cm^3/cm^3 initial water content and for water contents higher than 0.03 cm^3/cm^3 the matric potential is lower than further up in the "tail". There is a hyperbolic decay relationship between the initial water content and the matric potential difference between tip and tail ($R^2 = 99\%$).

The difference in water content at the wetting front and the "tail" also shows a hyperbolic relationship with the initial water content ($R^2 = 95\%$) (Fig. 8b). For initial water contents from 0–0.03 cm^3/cm^3 the water content is higher at the front than behind it, with the maximum difference for the initially air dry soil of 0.15 cm^3/cm^3. For 0.03 cm^3/cm^3 initial water, the water content remains constant and for initial water contents higher than 0.03 cm^3/cm^3 the moisture content increases behind the tip.

The matric potential data and moisture content data

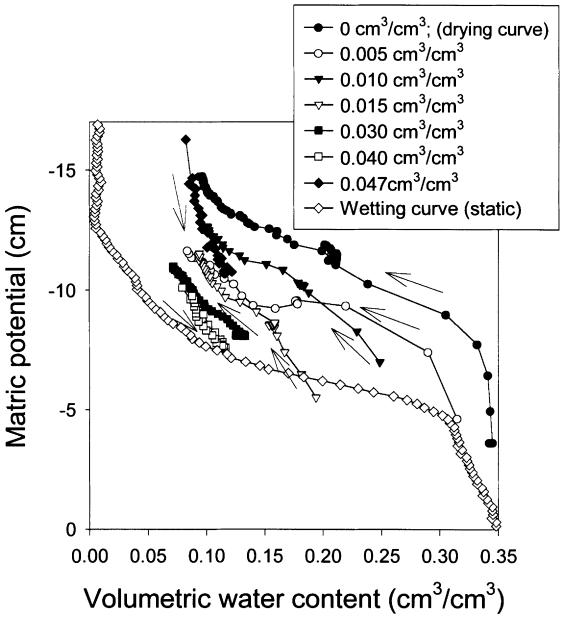

Fig. 9. The reconstituted parts of the wetting and drying curves determined from the measured volumetric water content and matric potential. Arrows indicate the direction the matric potential and moisture content changed just after the wetting front reached the measurement location (32 cm from the bottom). For the soils with initial water content of 0.04 and 0.047 cm^3/cm^3, the water content initially increased when the wetting front passed by (indicated with the arrows pointing to the right side).

in Figs. 7 and 8, together with the finger width data, shows that the fingers in air dry soil are "typical" unstable fingers as we have seen them in previous research (Glass et al., 1989; Selker et al., 1992b; Liu et al., 1994). The wetting front in the soil at field capacity (0.047 cm^3/cm^3) has the typical stable Richards' properties. The wetting front patterns for the other initial water contents have properties of both. The fingers in the 0.005 and 0.01 cm^3/cm^3 initial water contents have all the properties of an unstable wetting front, except that the moisture content at the front is not saturated. The fingers formed in the 0.02 and 0.03 cm^3/cm^3 initial water contents are intermediate between unstable and Richards': the fingers expand while the moisture content and matric potential are nearly independent of the position of the wetting front. For the 0.04 and 0.047 cm^3/cm^3 initial water contents, the fingers expand and moisture content and matric potential increase behind the front.

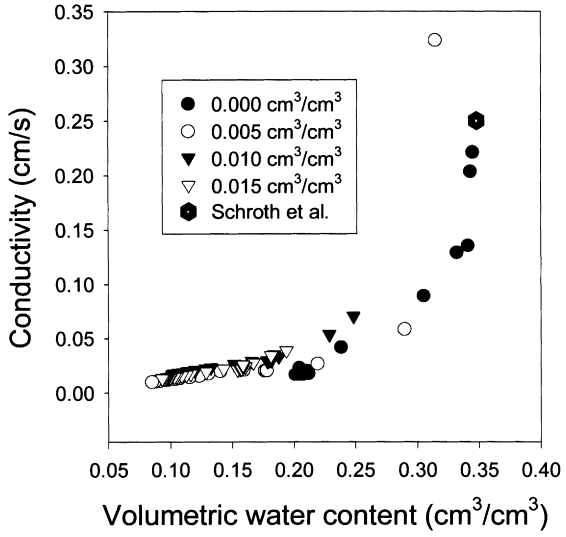

Fig. 10. Conductivity is plotted versus volumetric water content for the flow patterns that behave as an unstable wetting front. The saturated conductivity as calculated by Schroth et al. (1996) is also depicted.

3.3. Soil water properties

Because the pressure and matric potential were measured simultaneously, we can combine them to obtain the soil water characteristic curves (Fig. 9). Based on previous discussion, we expect that the moisture content and matric potential at the wetting front for unstable fingered flow are on the wetting curve and behind the front are on the drying curve. For the Richards' type front, the entire infiltration front is on the wetting curve. For the unstable front, the wetting curve is over such a short distance that it is impossible to measure. Only the static wetting curve for the initially dry soil is shown. The drying curves resulting from unstable fingered flow for the 0, 0.005, 0.01 and 0.015 cm^3/cm^3 initial moisture contents are shown in Fig. 9. Because the moisture contents at the wetting front are so different, they are each on a separate drying branch starting at the main wetting curve. The slight deviations are not significant because they are within the measuring error. The branch for the air dry sand is the main drying curve and is nearly identical to that obtained by Schroth et al. (1996). The branch obtained in the sand with 0.03 cm^3/cm^3 initial moisture content is also a drying curve obtained when the water started draining from the finger after the

water was turned off. It starts from the wetting front at a 0.13 cm^3/cm^3 moisture content. The branches obtained in the sand with 0.04 and 0.047 cm^3/cm^3 initial moisture content are wetting curves; since they were generated with a stable Richards' type wetting front. The procedure to obtain the two initial moisture contents was quite different. The 0.04 cm^3/cm^3 initial moisture content was obtained by mixing water with the sand and then put into the soil. Hence, this curve starts near the main wetting loop. The 0.047 cm^3/cm^3 initial moisture content was reached by saturating the sand and then draining to field capacity. Thus, this wetting branch should start at the main drying curve, which is indeed the case as shown in Fig. 9.

The fingered flow experiments allow us also to calculate the unsaturated conductivity as a function of moisture content. This can act as a check if the finger theory applies to the fingers at which the tip is not saturated. The theory is given in DiCarlo et al. (1999) and shortly summarized in Bauters et al. (2000). Fig. 10 shows that the calculated conductivity values for the different fingers all collapse to one line. Since conductivity is invariant of initial moisture content, this study shows that the fingered flow theory applies, indeed, nicely to unsaturated fingers.

4. Conclusions

The water content and matric potential at and behind the wetting front were measured systematically in a sand with water content increasing from air-dry to field capacity. The wetting front changed gradually from unstable to a stable Richards' type of wetting front. Consequently, three flow regimes can be distinguished: unstable, intermediate and stable Richards'. For unstable flow in air-dry sand, the finger does not widen, and there is a drop of pressure and water content behind the saturated tip. It is consistent with earlier theoretical postulates of Raats (1973) and Parlange and Hill (1976) that were experimentally confirmed by Selker et al. (1992a) and DiCarlo et al. (1999). For stable Richards' flow, the front moves both sideways and downwards and the pressure and water content increases behind the unsaturated wetting front. In the intermediate class, the fingers change gradually from unstable to stable Richards' type of wetting patterns. For increasing initial water contents, we found that the rate of expansion of the finger increased while the water content at the tip decreased. Moreover, a hyperbolic decay relationship existed between the initial water content and the difference between the tip and the steady state matric potential. A similar hyperbolic decay relation was found for the difference in water content between the front and the equilibrium water content that occurred far behind the front. The theory for the intermediate region has not been well developed. Future work should focus on the nature of the very fast lateral diffusion of the unstable phenomenon in initially moist soil.

Acknowledgements

We would like to thank Christophe Darnault, Qun Shen, and the staff at CHESS for useful discussions and experimental assistance. This research was supported (in part) by the Air Force Office of Scientific Research, USAF, under grant /contract number F49620-94-1-0291. CHESS is supported by NSF grant number DMR-931-1772.

References

Bauters, T.W.J., DiCarlo, D.A., Steenhuis, T.S., Parlange, J.-Y., 1998. Preferential flow in water repellent sands. Soil Sci. Soc. Am. J. 62, 1185–1190.

Bauters, T.W.J., Steenhuis, T.S., DiCarlo, D.A., Nieber, J.L., Dekker, L.W., Ritsema, C.J., Parlange, J.-Y., Haverkamp, R., 2000. Physics of water repellent soils. J. Hydrol. 231–232, 233–243.

Bruce, R.R., Klute, A., 1956. The measurement of soil water diffusivity. Soil Sci. Soc. Am. Proc. 20, 458–462.

DiCarlo, D.A., Bauters, T.W.J., Steenhuis, T.S., Parlange, J.-Y., Bierck, B.R., 1997. High-speed measurement of three-phase flow using synchrotron X rays. Water Resour. Res. 33, 569–576.

DiCarlo, D.A., Bauters, T.W.J., Darnault, C.J.G., Steenhuis, T.S., Parlange, J.-Y., 1999. Lateral expansion of preferential flow paths in sands. Water Resour. Res. 35, 427–434.

Diment, G.A., Watson, K.K., 1982. Stability analysis of water movement in unsaturated porous materials. 3. Experimental studies. Water Resour. Res. 21, 979–984.

Glass, R.J., Steenhuis, T.S., Parlange, J.-Y., 1989. Mechanism for finger persistence in homogenous, unsaturated, porous media: Theory and verification. Soil Sci. 148, 60–70.

Hill, D.E., Parlange, J.-Y., 1972. Wetting front instability in homogeneous soils. Soil Sci. Soc. Am. Proc. 36, 697–702.

Kapoor, V., 1996. Criterion for instability of steady-state unsaturated flows. Transport in Porous Media 25, 313–334.

Liu, Y., Steenhuis, T.S., Parlange, J.-Y., 1994. Formation and persistence of fingered flow fields in coarse grained soils under different moisture contents. J. Hydrol. 159, 187–195.

Miller, D.E., Gardner, W.H., 1962. Water infiltration into stratified soil. Soil Sci. Am. Proc. 26, 115–118.

Milly, P.C.D., 1988. Advances in modeling of water in the unsaturated zone. Transport in Porous Media 3, 491–514.

Parlange, J.-Y., Hill, D.E., 1976. Theoretical analysis of wetting front instability in soils. Soil Sci. 122, 236–239.

Peck, A.J., 1965. Moisture profile development and air compression during water uptake by bounded porous bodies. 3. Vertical columns. Soil Sci. 100, 44–51.

Raats, P.A.C., 1973. Unstable wetting fronts in uniform and nonuniform soils. Soil Sci. Soc. Am. Proc. 37, 681–685.

Ritsema, C.J., Dekker, L.W., Nieber, J.L., Steenhuis, T.S., 1998. Modeling and field evidence of finger formation and finger recurrence in a water repellent sandy soil. Water Resour. Res. 34, 555–567.

Schroth, M.H., Ahearn, S.J., Selker, J.S., Istok, J.D., 1996. Characterization of Miller-similar silica sands for laboratory hydrologic studies. Soil Sci. Soc. Am. J. 60, 1331–1339.

Selker, J.S., Leclerq, P., Parlange, J.-Y., Steenhuis, T.S., 1992a. Fingered flow in two dimensions. 1. Measurement of matric potential. Water Resour. Res. 28, 2513–2521.

Selker, J.S., Steenhuis, T.S., Parlange, J.-Y., 1992b. Fingered flow in two dimensions. 2. Predicting finger moisture profile. Water Resour. Res. 28, 2523–2528.

Yao, T.M., Hendrickx, J.M.H., 1996. Stability of wetting fronts in dry homogeneous soils under low infiltration rates. Soil Sci. Soc. Am. J. 60, 20–28.